meteorology

MDPI

Article

On the Human Thermal Load in Fog

Erzsébet Kristóf [1,*], Ferenc Ács [1] and Annamária Zsákai [2]

[1] Department of Meteorology, ELTE Eötvös Loránd University, H-1117 Budapest, Hungary; acs@staff.elte.hu
[2] Department of Human Anthropology, ELTE Eötvös Loránd University, H-1117 Budapest, Hungary; annamaria.zsakai@ttk.elte.hu
* Correspondence: ekristof86@staff.elte.hu

Abstract: We characterized the thermal load of a person walking and/or standing in the fog by analyzing the thermal resistance of clothing, r_{cl}, and operative temperature, T_o. The r_{cl}–T_o model applies to individuals using weather data. The body mass index and basal metabolic flux density values of the person analyzed in this study are 25 kg m^{-2} and 40 W m^{-2}, respectively. Weather data are taken from the nearest automatic weather station. We observed 146 fog events in the period 2017–2024 in Martonvásár (Hungary's Great Plain region, Central Europe). The main results are as follows: (1) The r_{cl} and T_o values were mostly between 2 and 0.5 clo and −4 and 16 °C during fog events, respectively. (2) The largest and smallest r_{cl} and T_o values were around 2.5 and 0 clo and −7 and 22 °C, respectively. (3) The r_{cl} differences resulting from interpersonal and wind speed variability are comparable, with a maximum value of around 0.5–0.7 clo. (4) Finally, r_{cl} values are significantly different for standing and walking persons. At the very end, we can emphasize that the thermal load of the fog depends noticeably on the person's activity and anthropometric characteristics.

Keywords: fog; human thermal load; thermal resistance of clothing; operative temperature; human data; Hungarian lowland; cold season

check for updates

Citation: Kristóf, E.; Ács, F.; Zsákai, A. On the Human Thermal Load in Fog. *Meteorology* **2024**, *3*, 83–96. https://doi.org/10.3390/meteorology3010004

Academic Editors: Edoardo Bucchignani and Paul D. Williams

Received: 30 November 2023
Revised: 14 January 2024
Accepted: 1 February 2024
Published: 6 February 2024

1. Introduction

In this study, we focus on the fog events of the Hungarian lowland, which are only typical in the cold season (autumn and winter). In Hungary, fog events have been analyzed in the past [1,2], but there is also a more recent analysis [3]. Analyses of fog are often climatological analyses [3–6], but there are also analyses in which the microphysical processes are investigated [7,8] or the relationships between fog, visibility [9], traffic [10], and air pollution [11] are analyzed. To the best of our knowledge, the human thermal load of fog has not been addressed so far.

Human thermal load is one of the central notions in human biometeorology. It expresses the energy flux density passing through the human body. Its unit is W m^{-2}. It should not be confused with the thermal sensation, even if they are correlated. During high thermal load (heat flux density reaching the body is much greater than 0), our thermal sensation is "warm", and conversely, during low thermal load (heat flux density reaching the body is around 0 or less than 0), our thermal sensation is "cold". The thermal sensation has no unit of measure; we categorize it. Human thermal load depends on both environmental and human factors. Since it depends on both factors, it must be calculated from the energy balance of the human body. There are many different methods for calculating the energy balance of the human body [12].

When examining the environmental thermal load, the researchers mostly dealt with the topics of human thermal comfort [13–15] and heat stress [16–18]. Nowadays, most of the research is conducted with models based on the energy balance of the human body [19]. The PET (Physiologically Equivalent Temperature) [20–22] and UTCI (Universal Thermal Climate Index) [23–26] are the most common indices. In the case of the PET index, the standard human is a 35-year-old man who has a body weight of 75 kg and a body length

of 175 cm; he is standing (metabolic heat flux density is about 80 W m^{-2}) in a room and possesses a typical indoor setting of 0.9 clo [27]. Clo is the unit for clothing insulation (1 clo = 0.155 m^2 °C W^{-1}). In the case of the UTCI index, the human has a body weight of 73.5 kg, a body fat content of 14%, and a Dubois area of 1.86 m^2; sex is not specified. This person is walking in outdoor conditions at a speed of 1.1 m s^{-1}. The person's clothing is estimated according to a clothing model [24], which represents the clothing patterns of European and North American urban populations. The clothing model is integrated into the UTCI-Fiala model [23]. In both methods, the humans presented are "reference humans"; thus, the sensitivity of human thermal load to human factors was not investigated. However, in some recent model applications [28], the concept of "reference human" is not applied; instead, anthropometric data of real persons were used. The main result of these investigations [29,30] is that human thermal load is significantly sensitive to the interpersonal variations in the anthropometric data in the case of a large environmental heat deficit.

Considering the above, this study has two objectives: (1) to provide a detailed analysis of human thermal load during fog events in the Hungarian lowland and (2) to investigate the sensitivity of human thermal load to changes in anthropometric data and human activity during fog events. The investigation is performed in the cold season in a lowland area of the Pannonian region (Hungary, Martonvásár) using a clothing thermal resistance–operative temperature model [28]. We chose this model because of its simplicity.

2. Materials and Methods

2.1. Clothing Thermal Resistance–Operative Temperature Model

The clothing thermal resistance–operative temperature model [29] is used for characterizing human thermal load. The philosophy of the model is old [31–34], the equation of clothing thermal resistance is new, and the equation of operative temperature and the parametrizations for calculating heat and air resistances were taken from Campbell and Norman's [35] and Fanger's [36] books. The model estimates the thermal insulation value of the imaginary clothing that ensures the thermal balance between the human body covered with clothing and its environment. The program for the model calculations was written in the Fortran programming language. The program, input files, and user manual are made available to users upon request.

We assume that (a) the human is covered by clothing completely, (b) the clothing's albedo is equal to the skin's albedo, (c) the clothing sticks strongly to the skin surface and the skin surface does not sweat, and (d) the human is walking at a speed of 1.1 m s^{-1}. The human body is represented as a single segment; that is, a one-node human body model is used [12]. The basic equation of the model characterizes the thermal resistance of the clothing r_{cl} [s m^{-1}], which can be estimated as follows:

$$r_{cl} = \rho \cdot c_p \cdot \frac{T_S - T_a}{M - \lambda E_{sd} - \lambda E_r - H_r - W} - r_{Hr} \cdot \left[\frac{R_{ni}}{M - \lambda E_{sd} - \lambda E_r - H_r - W} + 1 \right], \quad (1)$$

$$r_{cl} = \rho \cdot c_p \cdot \frac{T_S - T_o}{M - \lambda E_{sd} - \lambda E_r - H_r - W} - r_{Hr}, \quad (2)$$

In Equation (1), r_{cl} is expressed in terms of the isothermal net radiation, R_{ni} [W m^{-2}], whilst in Equation (2), it is expressed in terms of the operative temperature, T_o [°C]; ρ is the air density [kg m^{-3}]; c_p is the specific heat at constant pressure [J kg^{-1} $°C^{-1}$]; T_S is the skin temperature (34 °C) [35]; r_{Hr} is the combined resistance for expressing the thermal radiative and convective heat exchange effect [s m^{-1}]; and M is the metabolic heat flux density [W m^{-2}]. As mentioned, M refers to a walking person. λE_{sd} is the latent heat flux density of dry skin [W m^{-2}], λE_r is the respiratory latent heat flux density [W m^{-2}], H_r is the respiratory sensible heat flux density [W m^{-2}], and W is the mechanical work flux density [W m^{-2}]. It should be mentioned that r_{cl} is usually expressed in units of [clo]:

1 [clo] = 0.155 m^2 K W^{-1}. If $r_{cl}/(\rho \cdot c_p)$ = 1 [clo], then r_{cl} = 1.2 [kg m^{-3}] · 1004 [J kg^{-1} K^{-1}] · 0.155 [m^2 K W^{-1}] = 186.74 [s m^{-1}].

According to [37], a walking human's M can be expressed as

$$M = M_b + M_w, \tag{3}$$

where M_b is the basal metabolic rate [W] (sleeping human) and M_w is the metabolic rate [W] referring to walking. Both terms can be estimated if sex, age [year], body mass M_{bo} [kg], and body length L_{bo} [cm] of the human considered are known. Frankenfield et al. (2005) [38] state that the M_b parameterization in [39] is one of the best, which is the following

$$M_b^{\text{male}}\left[kcal \cdot day^{-1}\right] = 9.99 \cdot M_{bo} + 6.25 \cdot L_{bo} - 4.92 \cdot age + 5, \tag{4}$$

$$M_b^{\text{female}}\left[kcal \cdot day^{-1}\right] = 9.99 \cdot M_{bo} + 6.25 \cdot L_{bo} - 4.92 \cdot age - 161. \tag{5}$$

To be able to obtain M_b in [Wm^{-2}], the human body surface A [m^2] also has to be estimated. The parameterization in [40] is used for estimating A, taking M_{bo} and L_{bo} as inputs,

$$A = 0.2 \cdot M_{bo}^{0.425} \cdot \left(\frac{L_{bo}}{100}\right)^{0.725}. \tag{6}$$

M_w is parameterized according to [37] as follows:

$$M_w = 1.1 \cdot \frac{3.80 \cdot M_{bo} \cdot \left(\frac{L_{bo}}{100}\right)^{-0.95}}{A}. \tag{7}$$

λE_{sd}, λE_r, and H_r depend upon T_S or M; they are parameterized according to [41] as follows:

$$\lambda \mathrm{E}_{sd} = 3.05 \cdot 10^{-3} \cdot \left(256 \cdot T_s - 3373 - e_{ap}\right), \tag{8}$$

$$\lambda \mathrm{E}_r = 1.72 \cdot 10^{-5} \cdot \mathrm{M} \cdot \left(5867 - e_{ap}\right), \tag{9}$$

$$H_r = 1.4 \cdot 10^{-3} \cdot M \cdot (T_S - T_a), \tag{10}$$

where e_{ap} is actual vapor pressure [Pa], and T_a is air temperature [°C]. According to [32], W can be expressed as

$$W = 0.25 \cdot (M - M_b), \tag{11}$$

The combined resistance for expressing the thermal radiative and convective heat exchanges r_{Hr} is given by

$$\frac{1}{r_{Hr}} = \frac{1}{r_{Ha}} + \frac{1}{r_R} \text{ with}$$

$$r_{Ha}\left[sm^{-1}\right] = 7.4 \cdot 41 \cdot \sqrt{\frac{D}{U_{1.5}}}, \; \frac{1}{r_R} = \frac{4\epsilon_{cl}\sigma T_a^3}{\rho c_p}, \tag{12}$$

where D is the diameter of the cylindrical body used to approach the body of the observer [35], and $U_{1.5}$ is the wind speed at 1.5 m height (around breast height).

The operative temperature is an important environmental thermal load indicator. It depends upon the air temperature, the isothermal net radiation flux density, and the wind speed [35] as follows:

$$T_o = T_a + \frac{R_{ni}}{\rho \cdot c_p} \cdot r_{Hr}, \tag{13}$$

$$R_{ni} = S \cdot (1 - \alpha_{cl}) + \epsilon_a \sigma T_a^4 - \epsilon_{cl} \sigma T_a^4, \tag{14}$$

where S is the incoming solar radiation [W m^{-2}], σ is the Stefan-Boltzmann constant [W m^{-2} K^{-4}], ϵ_a is the emissivity of the cloudy sky, α_{cl} is the surface albedo of the clothing,

and ϵ_a and ϵ_{cl} are the emissivities of the atmosphere and clothing, respectively. In this study, α_{cl} = 0.27, like the surface of the skin, and $\epsilon_{cl} = 1$. S is estimated according to [42]

$$S = Q_0 \cdot [\alpha + (1 - \alpha) \cdot rsd], \tag{15}$$

where Q_0 is the solar radiation constant [MJ m^{-2} h^{-1}] referring to clear sky conditions and a 1 h time period, α is the corresponding dimensionless constant referring to the same hour, and rsd is the relative sunshine duration. ϵ_a depends on the clear sky emissivity, ϵ_{cs}, and the cloudiness N (0 for cloudless and 1 for completely overcast conditions),

$$\epsilon_a = \epsilon_{cs} \cdot \left(1 - N^{1.6}\right) + 0.9552 \cdot N^{1.6}, \tag{16}$$

$$\epsilon_{cs} = 0.51 + 0.066 \cdot \sqrt{e_a}. \tag{17}$$

ϵ_{cs} and ϵ_a are given according to [43,44], respectively.

The calculated values of R_{ni}, S, T_a, and r_{cl}—i.e., the output data—with respect to the fog observations can be found in Table S1 of the Supplementary Material.

2.2. Location

The region and the location of fog observations are presented in Figure 1. The town of Martonvásár (geographical latitude 47.31° N, geographical longitude 18.79° E) is located in the lowland area of the Central Transdanubian region of Hungary.

Figure 1. Topographical map of Hungary and Martonvásár (47.31° N, 18.79° E), the location of fog observations.

The climate of Martonvásár, according to Feddema, is "cool and dry with extreme variations of temperature" [45]. The mean annual clothing resistance is between 0.4 and 1 clo [46]. Fog appeared in the morning in the vast majority of cases. We documented our fog observations by collecting the following data: (1) the time of observing the fog (year, month, day, hour, minute) and (2) recording the values of meteorological elements. The radiation parameter (Q_0 and α) values are hourly values, and they refer to the hour interval during which the observation took place. The values of the other atmospheric state variables (air temperature, relative sunshine duration, cloud cover, wind gust speed, average wind speed, relative humidity, air pressure) are average values for a 10 min time interval. The data were written in a table in the order listed. These input data are available in Table S1 of the Supplementary Material.

2.3. Data

In this study, human and weather data are used.

2.3.1. Human Data

There is a Hungarian human data set that contains all relevant anthropometric data for more than 2000 Hungarian children and more than 1000 Hungarian adults [47–49]. Data needed to calculate M_b, body mass index BMI, and walking energy flux density are taken from this data set. The data set is the product of the Department of Biological Anthropology, Eötvös Loránd University, Budapest, Hungary.

In this study, we used the anthropometric data of 3 people; these can be seen in Table 1 together with M_b values calculated by Equation (4). We selected people based on their body mass and body length; age and sex were not considered. When selecting people, we tried to make the effect of individual variability noticeable. Now we are not dealing with the data of the "representative human". Such data are provided by Ács et al. [46].

Table 1. Anthropometric data of the 3 persons involved in this study.

Person	Sex	Age [Years]	Body Mass [kg]	Body Length [cm]	Basal Metabolic Heat Flux Density [W m^{-2}]
person 1	male	68	89	190	39.56
person 2	male	53	95	179	41.81
person 3	male	24	120	179	45.93

2.3.2. Weather Data

The thermal load of the air environment during fog events is estimated by using weather data. As mentioned, we used the following weather data: air temperature, relative sunshine duration, cloudiness, wind gust speed, average wind speed, relative humidity of air, and air pressure. All the elements, except relative sunshine duration and cloudiness, were measured by the automatic station of the private meteorological company Időkép, and these data were taken from their website https://www.idokep.hu/ (last accessed on 30 November 2023). The beeline distance between the station and the observer's location (garden of a family house) is shorter than 3 km. Cloud cover and relative sunshine duration data are provided by the observer. Cloud cover is estimated visually in tenths. Hourly radiation parameter (Q_0 and α) values are given in [42]. A total of 146 observations were made between 15 February 2017 and 2 January 2024. The observations were made on 97 foggy days.

The change in atmospheric state variables in the fog is very slow, and their values are typical or can be estimated. The relative sunshine duration is equal to 0, the cloud cover is equal to 1, the relative humidity is 100% or very close to this value, the air pressure is usually high, and the air movement is often very weak. Global radiation is also low but has a diurnal trend if the fog lasts all day. Among weather elements, the temperature and wind speed showed the greatest variations. The air temperature values during fog observations are presented in Figure 2.

We can see that the lowest air temperature values were around −5 °C and the highest around 12 °C. In the vast majority of cases, temperatures were between −2 °C and 10 °C.

The variations in wind gust speed and average wind speed values during fog observations are presented in Figure 3. Average wind speed values varied between 0.1 and 3.6 m s^{-1}. The value of 0.1 m s^{-1} means no wind. It should be emphasized that the value greater than 3 m s^{-1} occurred only once. In the majority of the cases, average wind speed values varied between 0.8 and 2 m s^{-1}; that is, the wind was weak. Wind gust speed values varied between 0.6 and 5.0 m s^{-1}, but in most cases, between 1 and 3 m s^{-1}. Logically, the relative humidity was around 100%, and the thermal load of radiation was low (global radiation values were under 180 W m^{-2}, and the highest radiant temperature values were 26 °C).

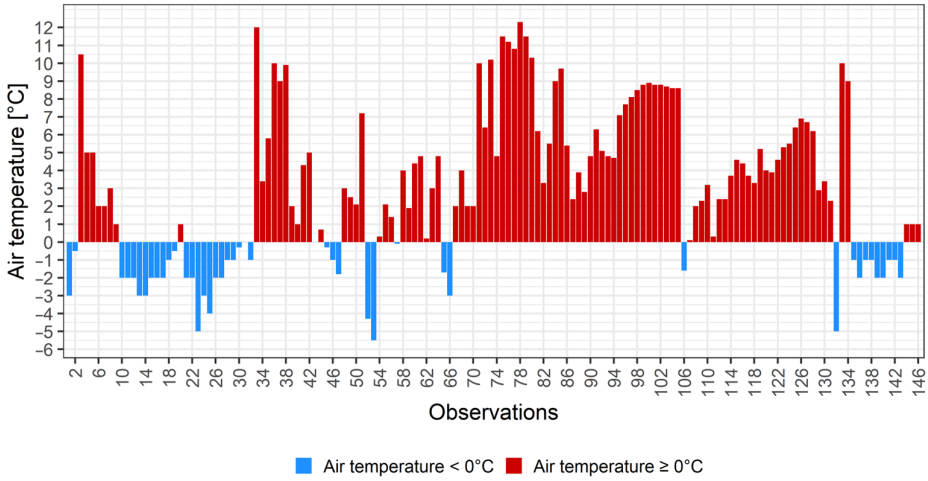

Figure 2. The 10 min mean air temperature values during fog observations in Martonvásár, Hungary. The sum of observations was 146, and these were made on 97 foggy days.

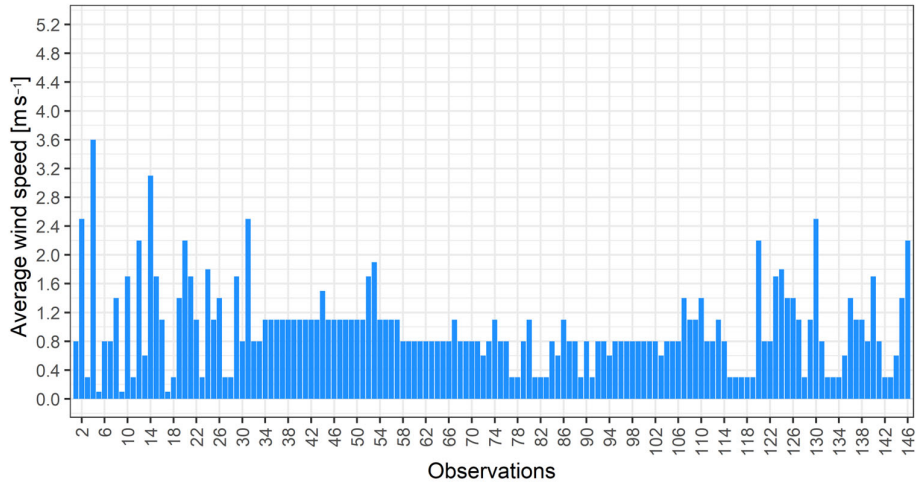

(**a**)

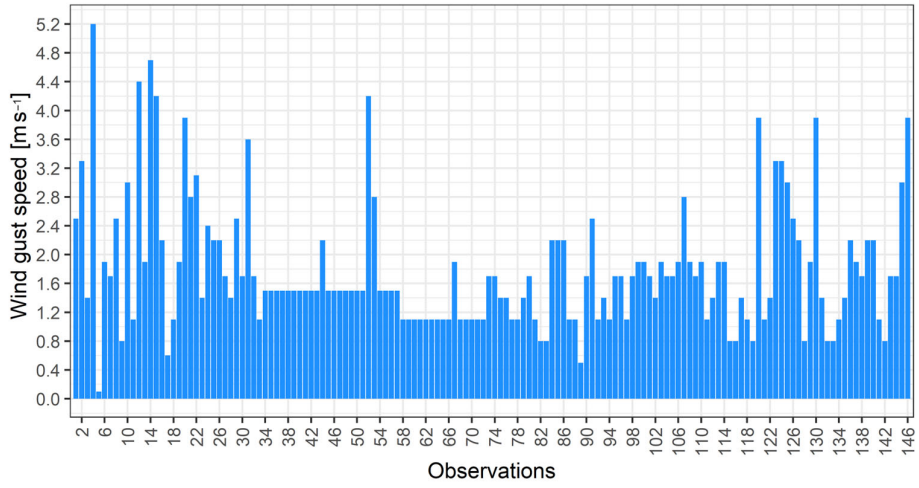

(**b**)

Figure 3. The 10 min (**a**) mean wind speed and (**b**) wind gust speed values during fog observations in Martonvásár, Hungary. The count of observations was 146, and these were made on 97 foggy days.

3. Results

The human thermal load results that characterize fog events are presented and described, highlighting the importance of human factors. First, we present the point cloud characterizing the M_b–BMI (body mass index) relationship for every person that is included in the Hungarian database, including the three featured persons (Table 1). Then, we characterize the relationship between r_{cl} and the operative temperature for person 1. After that, we characterize the impact of M on r_{cl}. Finally, we also analyzed the sensitivity of r_{cl} to wind speed variations.

3.1. The M_b–BMI Relationships

People's M_b–BMI relationship is an individual characteristic. The following question arises: how much does it vary from person to person? Regarding this, we can see an example in Figure 4. In Figure 4, we can see the dependence of the M_b values of more than 3000 men and women on the body mass index [48]. The magnitude of the scattering is about 20% for both men and women. It can also be seen that there is a systematic difference between the M_b values of men and women, the magnitude of which is around 5 W m^{-2}. This difference can be explained by the stronger physique of men. The M_b values of the three featured persons are marked with black dots. We can see that their M_b values are around 40–45 W m^{-2}, but their BMI values are much more scattered. We can also see that the BMI value of person 3 can be considered extreme since it is on the right edge of the point-cloud range.

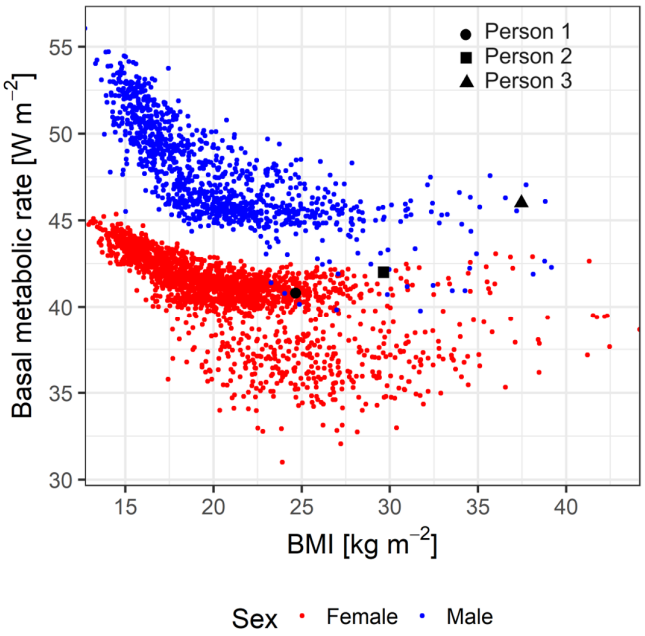

Figure 4. Point cloud representing the dependence of the basal metabolic heat flux density of men (blue) and women (red) on body mass index BMI. The points of persons 1 (circle), 2 (triangle), and 3 (cross) (Table 1) are marked in black. Sources of the data: Utczás et al. (2015), Zsákai and Bodzsár (2016), and Fehér et al. (2019); works [47–49].

3.2. Clothing Thermal Resistance and Operative Temperature Values Observed in the Fog

The human thermal load of the fog is analyzed by discussing the r_{cl}–T_o relationship. The point cloud of the r_{cl}–T_o relationship for person 1 can be seen in Figure 5.

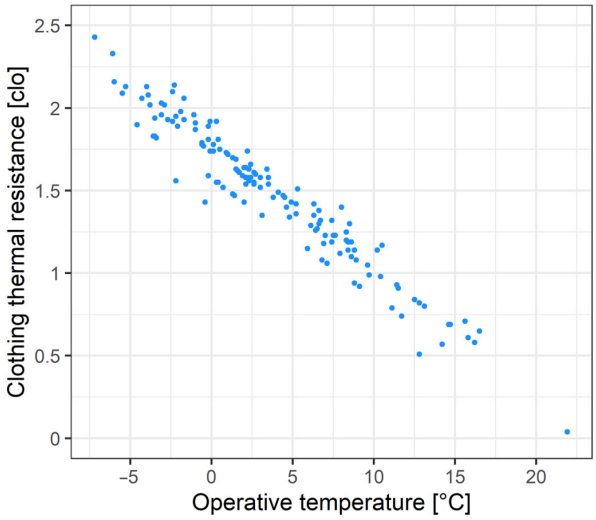

Figure 5. Scatter chart of the clothing thermal resistance of human 1 as a function of operative temperature; the human walks.

Each point in Figure 5 represents an observation. It should also be mentioned that this point cloud is individual-specific since r_{cl} depends on M. The r_{cl} values vary between 0 and 2.5 clo, but most of the points are scattered between 0.5 clo (T_o = 16 °C) and 2 clo (T_o = −4 °C). The fog that caused the smallest heat deficit was observed on October 20, 2017, at 10 am. Then, the estimated r_{cl} and T_o values are 0.05 clo and 21.9 °C, respectively. These values were caused by the higher air temperature (10.5 °C) and the slowly increasing radiation (S = 161 W m^{-2}, R_{ni} = 92 W m^{-2}). We did not register a fog event with a similarly small heat deficit (r_{cl} close to zero). In the other cases, the fog events with the smallest heat deficit were around 0.5 clo. In these cases, the air temperature (air temperature of about 7–8 °C) and irradiation conditions (S = 130 W m^{-2}, R_{ni} = 70 W m^{-2}) were lower. Fog events with a large heat deficit are above 2 clo. In these cases, the air temperature is mostly below 0 °C (it was only slightly higher than 0 °C in 2 cases), and the radiation balance of the human body is negative or close to zero (R_{ni} is between −30 and 10 W m^{-2}).

Fog events were usually registered in the morning hours. However, there were also days when we could observe the daily fluctuation in the heat deficit caused by the fog. We had three such days: 16 November and 23 December 2022, and 2 January 2023. The daily fluctuation in r_{cl} was best monitored on 16 November 2022. The daily changes in r_{cl}, R_{ni}, and S on 16 November are shown in Figure 6.

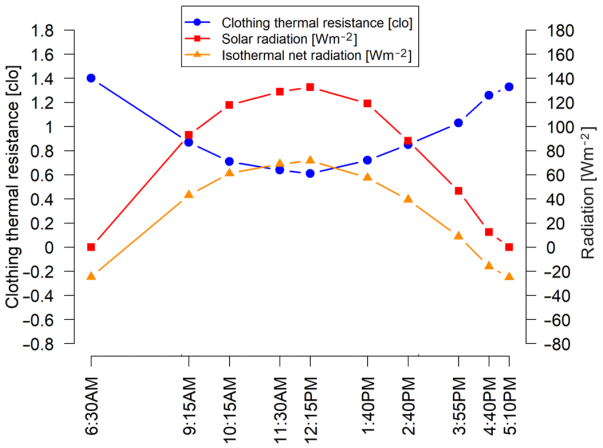

Figure 6. Daily variation in clothing thermal resistance for person 1 (blue curve with blue circles) and variation in incoming solar radiation (red curve with red rectangles) and isothermal net radiation orange curve with orange triangles) on 16 November 2022.

Air temperature fluctuates very little, between 7.7 and 8.9 °C. Thus, fluctuations in r_{cl}, which is around 0.8 clo, are determined by fluctuations in global radiation. However, note that S varies only between 0 and 133 Wm^{-2}. Since the range of registered r_{cl} values is mostly between 0.5 and 2 clo, the daily fluctuation of 0.8 clo cannot be considered small.

3.3. Sensitivity to Human Factors

The above results of r_{cl} refer to person 1, who is walking and has a walking speed of 1.1 m s^{-1}. The value of M obviously changes for different people or activities. In the following, we want to examine the sensitivity of r_{cl} to these two factors. A comparison of r_{cl} values obtained for humans 1, 2, and 3 when they are walking (the walking speed is 1.1 m s^{-1}) can be seen in Figure 7.

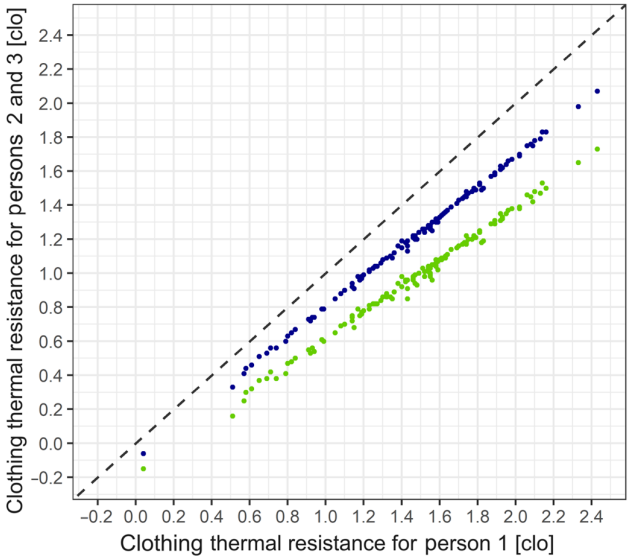

Figure 7. Comparison of clothing thermal resistance values referring to persons 2 and 1 (blue) and persons 3 and 1 (green); the persons are walking.

The comparison of persons 1 and 2 is indicated by blue dots, while the comparison between persons 1 and 3 is indicated by green dots. The difference in the *M* value between persons 1 and 2 and persons 1 and 3 is 15 and 35 W m^{-2}, respectively. Since person 1 has the smallest *M* value, the r_{cl} values of person 2 and person 3 are smaller than the r_{cl} values of person 1. The differences between the r_{cl} values vary between 0.2 and 0.7 clo, and we can see that they increase with increasing heat deficit. The maximum r_{cl} differences are between person 1 and person 3 when the heat deficit of person 1 is greater than 2 clo. Even bigger r_{cl} differences can be caused by differences in activity. We looked at the types of activity that occur most often outdoors: standing and walking. *M* for walking is estimated using Equations (3) and (7), while *M* for standing is estimated using the expression $M = 2.1 \cdot M_b$ [50,51]. Thus, the difference between the walking and standing *M* values obtained for person 1 is around 45–50 W m^{-2}. Such a difference in *M* values clearly separates the point clouds representing the r_{cl}–T_o relationship of a walking and a standing person. This is shown in Figure 8 for person 1. The differences between the r_{cl} values of a walking and a standing person increase as the heat deficit increases. The largest r_{cl} differences reach 2 clo (in the case of a large heat deficit), and the smallest differences are around 0.5 clo (in the case of a small heat deficit). In the middle of the T_o interval (T_o is about 2 °C), the difference between the r_{cl} values of the walking and standing person 1 is 1.5–1.8 clo.

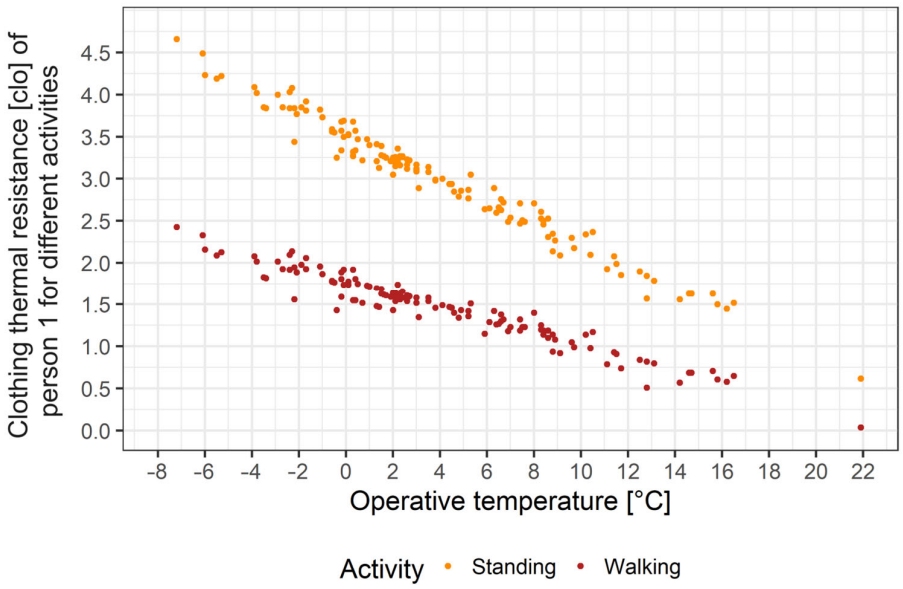

Figure 8. Scatter chart of the clothing thermal resistance of walking (red) and standing (orange) human 1 as a function of operative temperature.

3.4. Sensitivity to Wind Speed

The sensitivity of r_{cl} to changes in wind speed values is also tested. We applied two wind speed values: the wind gust speed and the average wind speed. The point cloud of r_{cl} values obtained for these wind speed values during fog events can be seen in Figure 9.

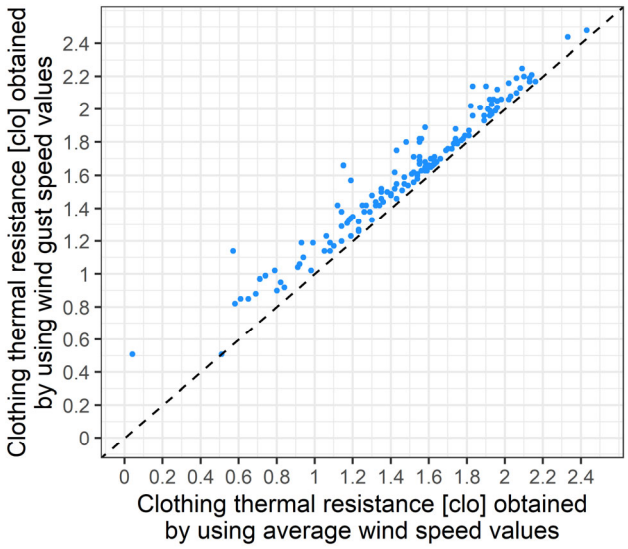

Figure 9. Scatter chart of the clothing thermal resistance values obtained by using wind gust speed and average wind speed values.

The r_{cl} values obtained for the values of the wind gust speed are, by definition, higher than the r_{cl} values obtained for the values of the average wind speed. These deviations in r_{cl} are larger in the case of a smaller heat deficit (r_{cl} is less than 1.2 clo), and in the majority of cases, they decrease as the heat deficit increases. The largest r_{cl} differences are around 0.5 clo, and the smallest differences are below 0.05 clo.

4. Discussion

As already mentioned, human thermal load depends on both environmental and human factors. Regarding environmental factors, special attention was paid to hazardous

weather phenomena such as heatwaves [52–54], cold stress weather [55,56], and weather associated with human mortality or morbidity [57,58]. In addition to extreme weather, biometeorological aspects of weather related to human well-being were also studied [25,59]. Today, energy-balance-based models are used in these studies. In these models, the human is either a "standardized human" or an individual. In scientific practice, the application of the "standardized human" is more widespread; he represents the selected human population. As a result, the role of human variability in human thermal load was not investigated at all. People differ not only in their anthropometric data but also in their clothing. The latter factor is completely individual, and it is culturally dependent; therefore, its variability is comparable to the variability of anthropometric data. Based on the above, we decided to use a clothing thermal resistance model using individual anthropometric data to eliminate the disadvantages mentioned above. This gave us the opportunity to compare the effects of the variability of weather and human factors on human thermal load.

Human thermal load during 146 fog events is analyzed in terms of r_{cl}–T_o relationship. To the best of our knowledge, there is no research in which fog has been characterized in terms of human thermal load. The main findings are as follows: (1) the r_{cl} values were mostly between 0.5 and 2 clo during fog observations; (2) the largest and smallest r_{cl} values were around 2.5 and 0 clo, respectively; (3) the median value of r_{cl} is 1.6 clo; and (4) the largest observed daily fluctuation in r_{cl} was around 0.8 clo, which is not a small value compared to the size of the observed r_{cl} range. These r_{cl} values were caused by fog. What r_{cl} values can be expected in the case of a clear sky on autumn or winter mornings? This question can only be answered if we estimate the r_{cl} values obtained in such cases. For this matter, we have such estimates, and if we compare the r_{cl} values obtained in this way (these are bigger) with the r_{cl} values obtained in the fog (these are smaller), we can obtain an estimate of how big the heating effect of the fog is. The r_{cl} values obtained in the case of clear sky varied between 0.9 and 3.5 clo. Only once was there a heat deficit of 4.1 clo. By definition, in these numerical experiments, the human (person 1) and the activity (walking at a speed of 1.1 m s^{-1}) were the same. Based on this, the heating effect of the fog can be roughly considered to be around 1 clo. Considering that the thermal insulation value of a suit is around 1 clo, this heating effect is considerable. This is obviously information that characterizes the climate of the lowland region of the Carpathian Basin; that is, it cannot be extended to other climates.

r_{cl} also depends on human factors. We used the anthropometric data of person 1 since its BMI and M_b values are located around the middle of the point cloud shown in Figure 4. We also investigated the effect of interpersonal variability on r_{cl}. We have shown that this effect (Figure 7) is comparable to the effect caused by wind speed variability (Figure 9). It should also be mentioned here that the average wind speed values experienced in fog are usually lower than 1.5 m s^{-1}. We have also shown that defining human activity and simulating it as accurately as possible is of fundamental importance when estimating human thermal load. We illustrated this by simulating the r_{cl} values of a walking and standing person (Figure 8). This effect is clearly stronger than the effect of interpersonal variability and increases in strength with increasing heat deficit. Figure 8 clearly proves that a person lying still has a much higher chance of getting cold or frozen than a moving person.

It should be mentioned that we did not perform thermal perception observations during the fog events. But we can also give an estimate based on [30]. In the case of the smallest heat deficit (r_{cl} around 0–0.8 clo), the thermal perception type is "cool" or even "neutral". In the case of moderate (r_{cl} 0.8–1.8 clo) heat deficit, the types of thermal sensation are "cool" or "cold", and in the case of a large (r_{cl} greater than 1.8 clo) heat deficit, "cold" or "very cold". The observer was always outside during fog observations, so his relationship with the fog was as direct as possible. From this point of view, we did not analyze the fog per se but the relationship between the person and the fog. This is confirmed by the sensitivity of the r_{cl}–T_o model to changes in human anthropometric data.

5. Conclusions

We dealt with the thermal load of a person walking or standing in fog. The thermal load is characterized by analyzing the r_{cl}–T_o relationship. The BMI and M_b values of the person are 25 kg m^{-2} and 40 W m^{-2}, respectively. The following main conclusions can be drawn: (1) in the majority of cases, the r_{cl} values were around 1.2–1.7 clo; (2) global radiation plays a decisive role in the daily changes in the thermal load of the fog despite the fact that the global radiation changes are small (between 0 and 180 W m^{-2}); (3) the differences between r_{cl} values caused by interpersonal variability and wind speed variability are comparable and are around 0.5–0.7 clo at most; and, lastly, (4) as the environmental heat deficit increases, the role of human activity in shaping the human thermal load also increases.

Supplementary Materials: The following supporting information can be downloaded at https://www.mdpi.com/article/10.3390/meteorology3010004/s1, Table S1: Input and output data.

Author Contributions: Conceptualization, F.Á.; methodology, F.Á. and A.Z.; software, F.Á. and E.K.; validation, F.Á.; formal analysis, F.Á.; investigation, F.Á., E.K. and A.Z.; resources, E.K.; data curation, F.Á. and A.Z.; writing—original draft preparation, F.Á.; writing—review and editing, E.K. and A.Z.; visualization, E.K.; supervision, F.Á. and A.Z.; project administration, E.K.; funding acquisition, E.K. All authors have read and agreed to the published version of the manuscript.

Funding: This research received no external funding.

Data Availability Statement: The original contributions presented in the study are included in the article and supplementary material, further inquiries can be directed to the corresponding author.

Conflicts of Interest: The authors declare no conflicts of interest.

References

1. Antal, E. The frequency of fog and its duration in different macrosynoptic situations (A köd gyakorisága és tartama a különböző makroszinoptikus helyzetekben in Hungarian). *Időjárás* **1958**, *62*, 39–45.
2. Kéri, M. The reflection of the metropolitan character in Budapest's foggy conditions (A nagyvárosi jelleg tükröződése Budapest ködviszonyaiban in Hungarian). *Időjárás* **1965**, *69*, 265–270.
3. Cséplő, A.; Sarkadi, N.; Horváth, Á.; Schmeller, G.; Lemler, T. Fog climatology in Hungary. *Időjárás* **2019**, *123*, 241–264. [CrossRef]
4. Bendix, J. Fog climatology of the Po Valley. *Riv. Meteorol. Aeronaut.* **1994**, *54*, 25–36.
5. Cermak, J.; Eastman, R.M.; Bendix, J.; Warren, S.G. European climatology of fog and low stratus based on geostationary satellite observations. *Q. J. R. Meteorol. Soc.* **2009**, *135*, 2125–2130. [CrossRef]
6. Egli, S.; Thies, B.; Drönner, J.; Cermak, J.; Bendix, J. A 10 year fog and low stratus climatology for Europe based on Meteosat Second Generation data. *Q. J. R. Meteorol. Soc.* **2017**, *143*, 530–541. [CrossRef]
7. Mensbrugghe, V. The formation of fog and of clouds, translated from Ciel et Terre. *Symons's Mon. Meteor. Mag.* **1892**, *27*, 40–41.
8. Weinstein, A.I.; Silverman, B.A. A numerical analysis of some practical aspects of airborne urea seeding for warm fog dispersal at airports. *J. Appl. Meteorol.* **1973**, *12*, 771–780. [CrossRef]
9. Wantuch, F. Visibility and fog forecasting based on decision tree method. *Időjárás* **2001**, *105*, 29–38.
10. Wu, Y.; Abdel-Aty, M.; Lee, J. Crash risk analysis during fog conditions using real-time traffic data. *Accid. Anal. Prev.* **2018**, *114*, 4–11. [CrossRef]
11. Zhu, Y.; Li, Z.; Zu, F.; Wang, H.; Liu, Q.; Qi, M.; Wang, Y. The propagation of fog and its related pollutants in the Central and Eastern China in winter. *Atmos. Res.* **2022**, *265*, 105914. [CrossRef]
12. Katić, K.; Li, R.; Zeiler, W. Thermophysiological models and their applications: A review. *Build. Environ.* **2016**, *106*, 286–300. [CrossRef]
13. Mayer, H.; Höppe, P.R. Thermal comfort of man in different urban environments. *Theor. Appl. Climatol.* **1987**, *38*, 43–49. [CrossRef]
14. Fröhlich, D.; Matzarakis, A. Modeling of changes in thermal bioclimate: Examples based on urban spaces in Freiburg, Germany. *Theor. Appl. Climatol.* **2013**, *111*, 547–558. [CrossRef]
15. Bröde, P.; Krüger, E.L.; Fiala, D. UTCI: Validation and practical application to the assessment of urban outdoor thermal comfort. *Geogr. Pol.* **2013**, *86*, 11–20. [CrossRef]
16. Schär, C.; Vidale, P.L.; Lüthi, D.; Frei, C.; Häberli, C.; Liniger, M.A.; Appenzeller, C. The role of increasing temperature variability in European summer heatwaves. *Nature* **2004**, *427*, 332–336. [CrossRef]
17. Matzarakis, A.; Mayer, H. Another kind of environmental stress: Thermal stress. *WHO Newsl.* **1996**, *18*, 7–10.
18. Matzarakis, A.; Mayer, H. Heat stress in Greece. *Int. J. Biometeorol.* **1997**, *41*, 34–39. [CrossRef]

19. Potchter, O.; Cohen, P.; Lin, T.P.; Matzarakis, A. Outdoor human thermal perception in various climates: A comprehensive review of approaches, methods and quantification. *Sci. Total Environ.* **2018**, *631–632*, 390–406. [CrossRef]
20. Höppe, P. *The Energy Balance in Humans (Original Title—Die Energiebilanz des Menschen)*; Universitat Munchen, Meteorologisches Institut: Munich, Germany, 1984.
21. Matzarakis, A.; Mayer, H.; Iziomon, M.G. Applications of a universal thermal index: Physiological equivalent temperature. *Int. J. Biometeorol.* **1999**, *43*, 76–84. [CrossRef]
22. Matzarakis, A.; Rutz, F.; Mayer, H. Modelling radiation fluxes in simple and complex environments—Application of the RayMan model. *Int. J. Biometeorol.* **2007**, *51*, 323–334. [CrossRef]
23. Fiala, D.; Havenith, G.; Bröde, P.; Kampmann, B.; Jendritzky, G. UTCI–Fiala multi-node model of human heat transfer and temperature regulation. *Int. J. Biometeorol.* **2011**, *56*, 429–441. [CrossRef]
24. Havenith, G.; Fiala, D.; Blazejczyk, K.; Richards, M.; Bröde, P.; Holmér, I.; Rintamaki, H.; Benshabat, Y.; Jendritzky, G. The UTCI-clothing model. *Int. J. Biometeorol.* **2012**, *56*, 461–470. [CrossRef]
25. Bröde, P.; Fiala, D.; Blazejczyk, K.; Holmér, I.; Jendritzky, G.; Kampmann, B.; Tinz, B.; Havenith, G. Deriving the operational procedure for the Universal Thermal Climate Index (UTCI). *Int. J. Biometeorol.* **2012**, *56*, 481–494. [CrossRef]
26. Błażejczyk, K.; Twardosz, R. Secular changes (1826–2021) of human thermal stress according to UTCI in Kraków (southern Poland). *Int. J. Climatol.* **2023**, *43*, 4220–4230. [CrossRef]
27. Höppe, P. The physiological equivalent temperature—A universal index for the biometeorological assessment of the thermal environment. *Int. J. Biometeorol.* **1999**, *43*, 71–75. [CrossRef]
28. Ács, F.; Szalkai, Z.; Kristóf, E.; Zsákai, A. Thermal Resistance of Clothing in Human Biometeorological Models. *Geogr. Pannonica* **2023**, *27*, 83–90. [CrossRef]
29. Ács, F.; Zsákai, A.; Kristóf, E.; Szabó, A.I.; Breuer, H. Human thermal climate of the Carpathian Basin. *Int. J. Climatol.* **2021**, *41*, E1846–E1859. [CrossRef]
30. Ács, F.; Kristóf, E.; Zsákai, A. Individual local human thermal climates in the Hungarian lowland: Estimations by a simple clothing resistance-operative temperature model. *Int. J. Climatol.* **2023**, *43*, 1273–1292. [CrossRef]
31. Auliciems, A.; de Freitas, C.R. Cold stress in Canada. A human climatic classification. *Int. J. Biometeorol.* **1976**, *20*, 287–294. [CrossRef]
32. Auliciems, A.; Kalma, J.D. A Climatic Classification of Human Thermal Stress in Australia. *J. Appl. Meteorol.* **1979**, *18*, 616–626. [CrossRef]
33. Yan, Y.Y. Climate Comfort Indices. In *Encyclopedia of World Climatology*; Oliver, J.E., Ed.; Springer: Dordrecht, The Netherlands, 2005; pp. 227–231. [CrossRef]
34. Yan, Y.Y.; Oliver, J.E. The Clo: A Utilitarian Unit to Measure Weather/Climate Comfort. *Int. J. Climatol.* **1996**, *16*, 1045–1056. [CrossRef]
35. Campbell, G.S.; Norman, J. *An Introduction to Environmental Biophysics*, 2nd ed.; Springer: New York, NY, USA, 1997; ISBN 978-0-387-94937-6.
36. Fanger, P.O. Thermal comfort. In *Analysis and Applications in Environmental Engineering*; Danish Technical Press: Copenhagen, Denmark, 1970.
37. Weyand, P.G.; Smith, B.R.; Puyau, M.R.; Butte, N.F. The mass-specific energy cost of human walking is set by stature. *J. Exp. Biol.* **2010**, *213*, 3972–3979. [CrossRef] [PubMed]
38. Frankenfield, D.; Roth-Yousey, L.; Compher, C. Comparison of Predictive Equations for Resting Metabolic Rate in Healthy Nonobese and Obese Adults: A Systematic Review. *J. Am. Diet. Assoc.* **2005**, *105*, 775–789. [CrossRef] [PubMed]
39. Mifflin, M.D.; St Jeor, S.T.; Hill, L.A.; Scott, B.J.; Daugherty, S.A.; Koh, Y.O. A new predictive equation for resting energy expenditure in healthy individuals. *Am. J. Clin. Nutr.* **1990**, *51*, 241–247. [CrossRef]
40. Dubois, D.; Dubois, E.F. The Measurement of the Surface Area of Man. *Arch. Intern. Med.* **1915**, *15*, 868–881. [CrossRef]
41. Thermal Comfort. Innova Air Tech Instruments A/S. 2002. Available online: http://www.labeee.ufsc.br/sites/default/files/disciplinas/Thermal%20Booklet.pdf (accessed on 2 February 2024).
42. Mihailović, D.T.; Ács, F. Calculation of daily amounts of global radiation in Novi Sad. *Időjárás* **1985**, *89*, 257–261. (In Hungarian)
43. Brunt, D. Notes on radiation in the atmosphere. *Q. J. R. Meteorol. Soc.* **1932**, *58*, 389–420. [CrossRef]
44. Konzelmann, T.; van de Wal, R.S.W.; Greuell, W.; Bintanja, R.; Henneken, E.A.C.; Abe-Ouchi, A. Parameterization of global and longwave incoming radiation for the Greenland Ice Sheet. *Glob. Planet. Chang.* **1994**, *9*, 143–164. [CrossRef]
45. Ács, F.; Breuer, H.; Skarbit, N. Climate of Hungary in the twentieth century according to Feddema. *Theor. Appl. Climatol.* **2015**, *119*, 161–169. [CrossRef]
46. Ács, F.; Kristóf, E.; Szabó, A.I.; Zsákai, A. New statistical deterministic method for estimating human thermal load and sensation—Application in the Carpathian region. *Theor. Appl. Climatol.* **2023**, *151*, 691–705. [CrossRef]
47. Utczás, K.; Zsákai, A.; Muzsnai, Á.; Fehér, V.P.; Bodzsár, É. The analysis of bone age estimations performed by radiological and ultrasonic methods in children aged between 7–17 years (Radiológiai és ultrahangos módszerrel végzett csontéletkor-becslések összehasonlító elemzése 7–17 éveseknél in Hungarian). *Anthrop. Közl.* **2015**, *56*, 129–138. [CrossRef]
48. Zsákai, A.; Bodzsár, É. The relationship between reproductive ageing and the changes of bone structure in women (A reprodukciós öregedés és csontszerkezet változásának kapcsolata nőknél in Hungarian). *Anthrop. Közl.* **2016**, *57*, 77–84. [CrossRef]

49. Fehér, V.P.; Annár, D.; Zsákai, A.; Bodzsár, É. The determinants of psychosomatic health complaints in 18–90 year-old women (Pszichoszomatikus tünetek gyakoriságát befolyásoló tényezők 18–90 éves nők körében in Hungarian). *Anthrop. Közl.* **2019**, *60*, 65–77. [CrossRef]
50. Di Napoli, C.; Pappenberger, F.; Cloke, H.L. Assessing heat-related health risk in Europe via the Universal Thermal Climate Index (UTCI). *Int. J. Biometeorol.* **2018**, *62*, 1155–1165. [CrossRef]
51. Amaro-Gahete, F.J.; Sanchez-Delgado, G.; Alcantara, J.M.A.; Martinez-Tellez, B.; Acosta, F.M.; Merchan-Ramirez, E.; Löf, M.; Labayen, I.; Ruiz, J.R. Energy expenditure differences across lying, sitting, and standing positions in young healthy adults. *PLoS ONE* **2019**, *14*, e0217029. [CrossRef]
52. Júdice, P.B.; Hamilton, M.T.; Sardinha, L.B.; Zderic, T.W.; Silva, A.M. What is the metabolic and energy cost of sitting, standing and sit/stand transitions? *Eur. J. Appl. Physiol.* **2016**, *116*, 263–273. [CrossRef] [PubMed]
53. Bašarin, B.; Lukić, T.; Matzarakis, A. Review of Biometeorology of Heatwaves and Warm Extremes in Europe. *Atmosphere* **2020**, *11*, 1276. [CrossRef]
54. Köppe, C.; Kovats, S.; Jendritzky, G.; Menne, B. *Heat Waves: Risks and Responses, No. 2*; Health and Global Environmental Change Series; World Health Organisation: Copenhagen, Denmark, 2004.
55. Holmér, I. Assessment of cold stress in terms of required clothing insulation—IREQ. *Int. J. Ind. Ergon.* **1988**, *3*, 159–166. [CrossRef]
56. Kuchcik, M.; Blażejczyk, K.; Halaś, A. Long-term changes in hazardous heat and cold stress in humans: Multicity study in Poland. *Int. J. Biometeorol.* **2021**, *65*, 1567–1578. [CrossRef] [PubMed]
57. Nastos, P.T.; Matzarakis, A. The effect of air temperature and human thermal indices on mortality in Athens, Greece. *Theor. Appl. Climatol.* **2012**, *108*, 591–599. [CrossRef]
58. Błażejczyk, A.; Błażejczyk, K.; Baranowski, J.; Kuchcik, M. Heat stress mortality and desired adaption responses of healthcare system in Poland. *Int. J. Biometeorol.* **2018**, *62*, 307–318. [CrossRef] [PubMed]
59. Błażejczyk, K.; Kunert, A. *Bioclimatic Principles of Recreation and Tourism in Poland (Bioklimatyczne Uwarunkowania Rekreacji i Turystyki w Polsce in Polish)*; Polish Academy of Sciences S. Leszczycki Institute of Geography and Spatial Organization: Warsaw, Poland, 2011; p. 365.